

Search for Radions at LEP2

The OPAL Collaboration

Abstract

A new scalar resonance, called the radion, with couplings to fermions and bosons similar to those of the Higgs boson, is predicted in the framework of Randall-Sundrum models, proposed solutions to the hierarchy problem with one extra dimension. An important distinction between the radion and the Higgs boson is that the radion would couple directly to gluon pairs, and in particular its decay products would include a significant fraction of gluon jets. The radion has the same quantum numbers as the Standard Model (SM) Higgs boson, and therefore they can mix, with the resulting mass eigenstates having properties different from those of the SM Higgs boson. Existing searches for the Higgs bosons are sensitive to the possible production and decay of radions and Higgs bosons in these models. For the first time, searches for the SM Higgs boson and flavour-independent and decay-mode independent searches for a neutral Higgs boson are used in combination to explore the parameter space of the Randall-Sundrum model. In the dataset recorded by the OPAL experiment at LEP, no evidence for radion or Higgs particle production was observed in any of those searches. The results are used to set limits on the radion and Higgs boson masses.

To be submitted to Physics Letters B

The OPAL Collaboration

G. Abbiendi², C. Ainsley⁵, P.F. Åkesson^{3,y}, G. Alexander²², J. Allison¹⁶, P. Amaral⁹,
G. Anagnostou¹, K.J. Anderson⁹, S. Asai²³, D. Axen²⁷, I. Bailey²⁶, E. Barberio^{8,p},
T. Barillari³², R.J. Barlow¹⁶, R.J. Batley⁵, P. Bechtel²⁵, T. Behnke²⁵, K.W. Bell²⁰,
P.J. Bell¹, G. Bella²², A. Bellerive⁶, G. Benelli⁴, S. Bethke³², O. Biebel³¹, O. Boeriu¹⁰,
P. Bock¹¹, M. Boutemour³¹, S. Braibant², R.M. Brown²⁰, H.J. Burckhart⁸, S. Campana⁴,
P. Capiluppi², R.K. Carnegie⁶, A.A. Carter¹³, J.R. Carter⁵, C.Y. Chang¹⁷,
D.G. Charlton¹, C. Ciocca², A. Csilling²⁹, M. Cuffiani², S. Dado²¹, A. De Roeck⁸, E.A. De
Wolf^{8,s}, K. Desch²⁵, B. Dienes³⁰, M. Donkers⁶, J. Dubbert³¹, E. Duchovni²⁴, G. Duckeck³¹,
I.P. Duerdoth¹⁶, E. Etzion²², F. Fabbri², P. Ferrari⁸, F. Fiedler³¹, I. Fleck¹⁰, M. Ford¹⁶,
A. Frey⁸, P. Gagnon¹², J.W. Gary⁴, C. Geich-Gimbel³, G. Giacomelli², P. Giacomelli²,
M. Giunta⁴, J. Goldberg²¹, E. Gross²⁴, J. Grunhaus²², M. Gruwé⁸, P.O. Günther³,
A. Gupta⁹, C. Hajdu²⁹, M. Hamann²⁵, G.G. Hanson⁴, A. Harel²¹, M. Hauschild⁸,
C.M. Hawkes¹, R. Hawkings⁸, R.J. Hemingway⁶, G. Herten¹⁰, R.D. Heuer²⁵, J.C. Hill⁵,
K. Hoffman⁹, D. Horváth^{29,c}, P. Igo-Kemenes¹¹, K. Ishii²³, H. Jeremie¹⁸, P. Jovanovic¹,
T.R. Junk^{6,i}, J. Kanzaki^{23,u}, D. Karlen²⁶, K. Kawagoe²³, T. Kawamoto²³, R.K. Keeler²⁶,
R.G. Kellogg¹⁷, B.W. Kennedy²⁰, S. Kluth³², T. Kobayashi²³, M. Kobel³, S. Komamiya²³,
T. Krämer²⁵, P. Krieger^{6,l}, J. von Krogh¹¹, T. Kuhl²⁵, M. Kupper²⁴, G.D. Lafferty¹⁶,
H. Landsman²¹, D. Lanske¹⁴, D. Lellouch²⁴, J. Letts^o, L. Levinson²⁴, J. Lillich¹⁰,
S.L. Lloyd¹³, F.K. Loebinger¹⁶, J. Lu^{27,w}, A. Ludwig³, J. Ludwig¹⁰, W. Mader^{3,b},
S. Marcellini², A.J. Martin¹³, G. Masetti², T. Mashimo²³, P. Mättig^m, J. McKenna²⁷,
R.A. McPherson²⁶, F. Meijers⁸, W. Menges²⁵, F.S. Merritt⁹, H. Mes^{6,a}, N. Meyer²⁵,
A. Michelini², S. Mihara²³, G. Mikenberg²⁴, D.J. Miller¹⁵, W. Mohr¹⁰, T. Mori²³,
A. Mutter¹⁰, K. Nagai¹³, I. Nakamura^{23,v}, H. Nanjo²³, H.A. Neal³³, R. Nisius³²,
S.W. O’Neale^{1,*}, A. Oh⁸, M.J. Oreglia⁹, S. Orito^{23,*}, C. Pahl³², G. Pásztor^{4,g}, J.R. Pater¹⁶,
J.E. Pilcher⁹, J. Pinfold²⁸, D.E. Plane⁸, O. Pooth¹⁴, M. Przybycień^{8,n}, A. Quadt³,
K. Rabbertz^{8,r}, C. Rembser⁸, P. Renkel²⁴, J.M. Roney²⁶, A.M. Rossi², Y. Rozen²¹,
K. Runge¹⁰, K. Sachs⁶, T. Saeki²³, E.K.G. Sarkisyan^{8,j}, A.D. Schaile³¹, O. Schaile³¹,
P. Scharff-Hansen⁸, J. Schieck³², T. Schörner-Sadenius^{8,z}, M. Schröder⁸, M. Schumacher³,
R. Seuster^{14,f}, T.G. Shears^{8,h}, B.C. Shen⁴, P. Sherwood¹⁵, A. Skuja¹⁷, A.M. Smith⁸,
R. Sobie²⁶, S. Söldner-Rembold¹⁶, F. Spano⁹, A. Stahl^{3,x}, D. Strom¹⁹, R. Ströhmer³¹,
S. Tarem²¹, M. Tasevsky^{8,s}, R. Teuscher⁹, M.A. Thomson⁵, E. Torrence¹⁹, D. Toya²³,
P. Tran⁴, I. Trigger⁸, Z. Trócsányi^{30,e}, E. Tsur²², M.F. Turner-Watson¹, I. Ueda²³,
B. Ujvári^{30,e}, C.F. Vollmer³¹, P. Vannerem¹⁰, R. Vértesi^{30,e}, M. Verzocchi¹⁷, H. Voss^{8,q},
J. Vossebeld^{8,h}, C.P. Ward⁵, D.R. Ward⁵, P.M. Watkins¹, A.T. Watson¹, N.K. Watson¹,
P.S. Wells⁸, T. Wengler⁸, N. Wermes³, G.W. Wilson^{16,k}, J.A. Wilson¹, G. Wolf²⁴,
T.R. Wyatt¹⁶, S. Yamashita²³, D. Zer-Zion⁴, L. Zivkovic²⁴

¹School of Physics and Astronomy, University of Birmingham, Birmingham B15 2TT, UK

²Dipartimento di Fisica dell’ Università di Bologna and INFN, I-40126 Bologna, Italy

³Physikalisches Institut, Universität Bonn, D-53115 Bonn, Germany

⁴Department of Physics, University of California, Riverside CA 92521, USA

⁵Cavendish Laboratory, Cambridge CB3 0HE, UK

⁶Ottawa-Carleton Institute for Physics, Department of Physics, Carleton University, Ottawa, Ontario K1S 5B6, Canada

- ⁸CERN, European Organisation for Nuclear Research, CH-1211 Geneva 23, Switzerland
- ⁹Enrico Fermi Institute and Department of Physics, University of Chicago, Chicago IL 60637, USA
- ¹⁰Fakultät für Physik, Albert-Ludwigs-Universität Freiburg, D-79104 Freiburg, Germany
- ¹¹Physikalisches Institut, Universität Heidelberg, D-69120 Heidelberg, Germany
- ¹²Indiana University, Department of Physics, Bloomington IN 47405, USA
- ¹³Queen Mary and Westfield College, University of London, London E1 4NS, UK
- ¹⁴Technische Hochschule Aachen, III Physikalisches Institut, Sommerfeldstrasse 26-28, D-52056 Aachen, Germany
- ¹⁵University College London, London WC1E 6BT, UK
- ¹⁶Department of Physics, Schuster Laboratory, The University, Manchester M13 9PL, UK
- ¹⁷Department of Physics, University of Maryland, College Park, MD 20742, USA
- ¹⁸Laboratoire de Physique Nucléaire, Université de Montréal, Montréal, Québec H3C 3J7, Canada
- ¹⁹University of Oregon, Department of Physics, Eugene OR 97403, USA
- ²⁰CCLRC Rutherford Appleton Laboratory, Chilton, Didcot, Oxfordshire OX11 0QX, UK
- ²¹Department of Physics, Technion-Israel Institute of Technology, Haifa 32000, Israel
- ²²Department of Physics and Astronomy, Tel Aviv University, Tel Aviv 69978, Israel
- ²³International Centre for Elementary Particle Physics and Department of Physics, University of Tokyo, Tokyo 113-0033, and Kobe University, Kobe 657-8501, Japan
- ²⁴Particle Physics Department, Weizmann Institute of Science, Rehovot 76100, Israel
- ²⁵Universität Hamburg/DESY, Institut für Experimentalphysik, Notkestrasse 85, D-22607 Hamburg, Germany
- ²⁶University of Victoria, Department of Physics, P O Box 3055, Victoria BC V8W 3P6, Canada
- ²⁷University of British Columbia, Department of Physics, Vancouver BC V6T 1Z1, Canada
- ²⁸University of Alberta, Department of Physics, Edmonton AB T6G 2J1, Canada
- ²⁹Research Institute for Particle and Nuclear Physics, H-1525 Budapest, P O Box 49, Hungary
- ³⁰Institute of Nuclear Research, H-4001 Debrecen, P O Box 51, Hungary
- ³¹Ludwig-Maximilians-Universität München, Sektion Physik, Am Coulombwall 1, D-85748 Garching, Germany
- ³²Max-Planck-Institute für Physik, Föhringer Ring 6, D-80805 München, Germany
- ³³Yale University, Department of Physics, New Haven, CT 06520, USA

^a and at TRIUMF, Vancouver, Canada V6T 2A3

^b now at University of Iowa, Dept of Physics and Astronomy, Iowa, U.S.A.

^c and Institute of Nuclear Research, Debrecen, Hungary

^e and Department of Experimental Physics, University of Debrecen, Hungary

^f and MPI München

^g and Research Institute for Particle and Nuclear Physics, Budapest, Hungary

^h now at University of Liverpool, Dept of Physics, Liverpool L69 3BX, U.K.

ⁱ now at Dept. Physics, University of Illinois at Urbana-Champaign, U.S.A.

^j and Manchester University

^k now at University of Kansas, Dept of Physics and Astronomy, Lawrence, KS 66045, U.S.A.

^l now at University of Toronto, Dept of Physics, Toronto, Canada

- ^m current address Bergische Universität, Wuppertal, Germany
- ⁿ now at University of Mining and Metallurgy, Cracow, Poland
- ^o now at University of California, San Diego, U.S.A.
- ^p now at The University of Melbourne, Victoria, Australia
- ^q now at IPHE Université de Lausanne, CH-1015 Lausanne, Switzerland
- ^r now at IEKP Universität Karlsruhe, Germany
- ^s now at University of Antwerpen, Physics Department, B-2610 Antwerpen, Belgium; supported by Interuniversity Attraction Poles Programme – Belgian Science Policy
- ^u and High Energy Accelerator Research Organisation (KEK), Tsukuba, Ibaraki, Japan
- ^v now at University of Pennsylvania, Philadelphia, Pennsylvania, USA
- ^w now at TRIUMF, Vancouver, Canada
- ^x now at DESY Zeuthen
- ^y now at CERN
- ^z now at DESY
- * Deceased

1 Introduction

In [?], a model was proposed to solve the problem of the hierarchy between the electroweak mass scale, $\Lambda_W = \mathcal{O}(\text{TeV})$, and the Planck mass $M_{\text{Pl}} = \mathcal{O}(10^{15} \text{TeV})$ at which gravity becomes strong. In this model, the hierarchy is generated by extending four-dimensional space time with compact extra dimensions. In the resulting effective four-dimensional theory, M_{Pl} appears enlarged with respect to the hypothesised fundamental value $\widetilde{M}_{\text{Pl}}$, due to the hidden volume V_n of the n extra dimensions: $M_{\text{Pl}}^2 = \widetilde{M}_{\text{Pl}}^{2+n} V_n$. To generate the observed value $\widetilde{M}_{\text{Pl}} = 10^{15} \text{TeV}$ from a hypothesised fundamental value close to the electroweak scale, $\widetilde{M}_{\text{Pl}} \simeq 1 \text{TeV}$, many additional dimensions are necessary or each additional dimension must be extraordinarily large, which generally conflicts with constraints from electroweak precision measurements. The constraints do not directly apply if the electroweak and strong forces and the particles of the Standard Model (SM) are confined to a four-dimensional subspace (brane), and only gravity is allowed to propagate into the whole space. Measurements of the gravitational force limit the size of extra dimensions to $200 \mu\text{m}$ [?]. Model dependent constraints can be obtained from electroweak precision observables, which can be affected in a sizable way by gravity [?].

In the Randall-Sundrum (RS) model [?], one compact extra dimension is introduced. As in previous models, the extra dimension is hidden to the forces and particles of the SM by confining them to one brane, the SM brane. Only gravity is allowed to propagate into the extra dimension. In this model the hierarchy is not generated by the extra volume, but by a specifically chosen “warped” geometry. As a direct consequence of the geometry, gravity is mainly located close to a second brane, the Planck brane, which is located at a distance r_0 away from the SM brane, and its propagation in the extra dimension is exponentially damped. Thus, there is only a small overlap between gravity and SM particles and forces, explaining the weakness of gravity with respect to the electroweak interaction, i.e. the observed mass hierarchy. The constraints on the size of the extra dimensions do not apply in this case, because the gravitational force is only weakly modified due to the localisation of gravity.

The model is considered to be a low-energy approximation of a more fundamental theory and does not explain the mechanism that traps the SM fields on the brane or the mechanism which gives rise to the geometry. It is possible to derive models with such a geometry from M-theory [?].

The spectrum of the additional particles in the RS model has been investigated in [?] and [?]. There are massless and massive spin-two excitations. The massless excitations couple with gravitational strength and can be identified with gravitons. The masses and couplings of the massive spin-two excitations are set by the weak scale. These states have not been observed, but if they exist, they should be observable at experiments using the next generation of colliders. In addition, there is a spinless excitation, called the *radion*. The radion corresponds to a local fluctuation of the inter-brane distance: $r_0 \rightarrow r_0 + \Delta r(x)$. To prevent the branes from drifting apart faster than allowed by cosmological models, a stabilisation mechanism is needed [?]. As a consequence, the radion acquires a mass [?]. To introduce no further hierarchies, the mass should be well below 1 TeV.

The radion carries the same quantum numbers as the Higgs boson; thus the radion and

the Higgs boson can mix. This possibility was investigated first in [?] and was pursued in [?], where calculations are carried out to higher order. The present study is based on the Lagrangian of [?]. The physical scalars of the model are derived therein. The couplings to matter are investigated in [?], where the calculations are based on a Lagrangian of a lower order approximation. The ideas of [?] are transferred to the Lagrangian of [?] leading to the results summarised in Section 2. The derivation of the physical scalars and the couplings to matter are detailed in the Appendices A.1 and A.2.

Like the SM Higgs boson, both scalars are mainly produced in the ‘‘Higgsstrahlung’’ process, $e^+e^- \rightarrow Zr$ or Zh , at LEP2, where r and h are the two scalar mass eigenstates of the model. The limits on the cross-section of the Higgsstrahlung process obtained from searches for the SM Higgs boson, flavour independent searches for hadronically decaying Higgs bosons and decay-mode independent searches for Higgs bosons are used to restrict the parameter space of the Randall-Sundrum model as explained in Section 3.

2 The Scalars of the Randall-Sundrum Model

In the Randall-Sundrum model there are two scalar particles, the radion and the Higgs boson. Their masses, m_r and m_h , are free parameters. Further free parameters are: Λ_W , which sets the mass scale on the SM brane and is expected to be $\mathcal{O}(1 \text{ TeV})$, and ξ which controls the kinematic mixing between the radion and the Higgs boson.

The radion couples to the trace of the energy momentum tensor. Thus, to first order the radion couples to massive particles with couplings proportional to the particle mass, and the Lorentz structure of the couplings is identical to that of the Higgs boson. However, the coupling strength of the radion is generally reduced by $v/\sqrt{6}\Lambda_W$ w.r.t. the couplings of the SM Higgs boson, where v denotes the vacuum expectation value of the Higgs field. Unlike the Higgs boson, which only couples to gluons via a top loop, the radion couples directly to gluon pairs due to the anomaly of the trace of the energy momentum tensor. As a consequence, the radion decays mostly into gluon pairs.

Due to the kinematic mixing of the radion and the Higgs boson, both physical scalars, the Higgs-like and the radion-like state h and r , may have properties different from those of the SM Higgs boson. Here, the radion-like and the Higgs-like states, $r(\xi)$ and $h(\xi)$, are defined such that the Higgs-like state becomes the SM Higgs boson in the limit $\xi \rightarrow 0$, and the mapping between the fundamental mass parameters (the mass parameter of the Higgs mechanism, \tilde{m}_h , and the mass parameter assigned to the radion excitation, \tilde{m}_r) to the mass eigenvalues is a continuous function of ξ (see Figure 1a and Appendix A.1 for details).

For non-zero mixing ($\xi \neq 0$) some combinations of the masses m_r and m_h of the radion-like and the Higgs-like state will lead to unphysical particles (ghosts or tachyons). The allowed minimum and maximum mixing is limited by requiring the particles to be physical. The limits depend on the masses, m_r and m_h , and the mass scale Λ_W . For fixed masses, the bounds increase with Λ_W . The physical regions are displayed in Figure 1b as a function of the mixing parameter ξ , and m_r for one Λ_W and m_h .

Both particles, the radion and the Higgs boson, are predominantly produced in “Higgsstrahlung” in e^+e^- collisions for masses in the range accessible by the LEP experiments. The production of the radion-like and the Higgs-like states are complementary as seen in Figure 2a and b. The branching ratio of the Higgs-like state into heavy quarks and leptons may be reduced depending on the mixing parameter ξ while the branching ratio into gluon pairs is enhanced, which can be seen in Figure 2c and d. Therefore, searches for the SM Higgs boson (assuming $m_{\text{HSM}} \ll 2m_W$) which are sensitive only to the decay mode $h \rightarrow b\bar{b}$, may lose their sensitivity, in contrast to flavour independent searches which are sensitive to $h \rightarrow gg$.

3 Experimental Constraints on the Randall-Sundrum Model

Since the signatures of the radion-like and the Higgs-like states are similar to the signatures of the SM Higgs boson or neutral Higgs bosons of more general models, searches for a neutral Higgs boson also constrain the parameter space of the Randall-Sundrum (RS) model. The following searches for the Higgsstrahlung process, $e^+e^- \rightarrow Z\varphi$, are exploited, where φ is a scalar:

1. The search for the SM Higgs boson [?], $\varphi = \text{H}_{\text{SM}}$, which exploits the properties of the dominant decay mode of the SM Higgs boson, $\text{H}_{\text{SM}} \rightarrow b\bar{b}$ (assuming $m_{\text{HSM}} \ll 2 \times m_W$). The decay $\text{H}_{\text{SM}} \rightarrow \tau^+\tau^-$ is not considered here. The search uses 593 pb^{-1} and 170 pb^{-1} of data collected with the OPAL detector at $\sqrt{s} = 189 - 209 \text{ GeV}$ and $\sqrt{s} = 91 \text{ GeV}$, respectively. All possible decay modes of the Z boson are considered: $Z \rightarrow q\bar{q}, e^+e^-, \mu^+\mu^-, \tau^+\tau^-$ and $\nu\bar{\nu}$.
2. A flavour independent search for hadronically decaying Higgs bosons, $\varphi = h$, sensitive to the $h \rightarrow q\bar{q}$ and $h \rightarrow gg$ modes, using the same dataset as above [?].
3. A search [?], independent of the decay mode of the scalar particle, using events in which the Z boson decays into muon or electron pairs. There are no assumptions on the scalar particle decay. Although this search gives weaker limits than the two above, it is the only search to cover the mass region from 1 MeV to 12 GeV.

These searches have not revealed any significant excess of data over the background from Standard Model processes, and limits on the cross-section of the Higgsstrahlung process times the branching ratio of the scalar particle decay have been derived at the 95% confidence level. The limits are expressed in terms of a scaling factor $k_{\varphi x}^{95}$, which relates the maximally allowed cross-section times branching ratio, $\sigma_{\varphi Z}^{95}(m_\varphi) \times \text{Br}(\varphi \rightarrow x\bar{x})$, of a scalar particle φ to the expectation for Higgs boson production $\sigma_{\text{HZ}}^{\text{SM}}(m_\varphi)$ from the SM:

$$k_{\varphi x}^{95}(m_\varphi) = \frac{\sigma_{\varphi Z}^{95}(m_\varphi)}{\sigma_{\text{HZ}}^{\text{SM}}(m_\varphi)} \times \text{Br}(\varphi \rightarrow x\bar{x}) \quad (1)$$

A value $k_{\varphi x}^{95}(m_{\varphi x}) = 1$ means that at the 95% confidence level, a cross-section could be excluded which is equal to the cross-section of the Higgsstrahlung process, $e^+e^- \rightarrow \text{H}_{\text{SM}}Z$,

for a SM Higgs boson H_{SM} having the mass m_φ . The observed and expected limits are depicted in Figure 3. The first search is sensitive only to $\varphi \rightarrow b\bar{b}$, the second to $\varphi \rightarrow q\bar{q}$, $\varphi \rightarrow gg$, and the third analysis covers all possible decays.

In the RS model, the radion-like and the Higgs-like states have the same coupling structure as a SM Higgs boson. The couplings to fermions f or vector bosons V only differ by factors $\sqrt{k_f}$ or $\sqrt{k_V}$ which depend on the masses of the radion-like and the Higgs-like states, m_r and m_h , the mixing parameter ξ , and the mass scale Λ_W (see Appendix A.2). Thus, the limits $k_{\varphi x}^{95}$ apply to the processes predicted in the RS model, $e^+e^- \rightarrow Z\varphi$, where φ is the radion-like state r or the Higgs-like state h .

Points in the parameter space of the RS model are considered excluded if the predicted cross-section times branching ratio for either the radion-like or the Higgs-like state exceeds the limit obtained from one of the Higgs boson searches. At each scan point, the search is chosen which yields the most restrictive expected limit. For example in Figures 4a-d, the cross-sections times branching ratio of the radion-like and Higgs-like state are shown together with the limit obtained from the flavour independent and the SM Higgs boson search. For the model points of Figures 4a and b, a small region in the parameter space just before the inaccessible region remains allowed. Neither the SM nor the flavour independent Higgs boson search is able to exclude this region. For the parameters shown in Figure 4c, the SM search is not capable of excluding the model points for the parameters $\xi = 0.25$, $\Lambda_W = 300 \text{ GeV}$, $m_h = 120 \text{ GeV}$, and for masses of the radion-like state $m_r \lesssim 67 \text{ GeV}$. The flavour independent Higgs boson search excludes all model points up to the inaccessible region (Figure 4d).

To find the lowest masses compatible with the observations, scans over the parameter space of the RS model are performed. Figures 5a and b show the lowest mass of the Higgs-like state allowed at the 95% confidence level in the plane spanned by the mixing parameter ξ and the scale parameter Λ_W . In the ξ -direction an equidistant grid is chosen using 200 points between the minimum and maximum value of the allowed region. In the Λ_W -direction, 160 scan points are chosen equally spaced on a logarithmic scale from 246 GeV to 10 TeV. At each scan point, m_r is scanned initially in coarse steps in the range from 1 MeV to 1 TeV, where the step sizes are 1 – 3 GeV and 30 GeV below and above 400 GeV, respectively. For each m_r value, m_h is scanned in the range from 1 MeV to 120 GeV in steps of 1 GeV. The scan stops if the predicted cross-section times branching ratio of both the radion-like and the Higgs-like states drops below the limit of the most sensitive Higgs boson search. Finally, the mass m_h at which the cross-section drops below the limit is found to within 250 MeV by an iterative procedure.

For zero mixing ($\xi = 0$), the mass limit of the SM Higgs boson search is obtained. For non-zero mixing, the mass limit of the Higgs-like state is generally lower and decreasing with decreasing scale parameter Λ_W . The lowest mass limits are generally obtained for maximum or minimum values of ξ and values of the radion mass much larger than the limit on m_h . In Figure 6 the lowest mass limits of the Higgs-like states are shown for all ξ allowed by the theory. At large Λ_W , the maximally allowed $|\xi|$ is beyond $\mathcal{O}(1)$. For all ξ , m_r and Λ_W , the Higgs mass has to be larger than 58 GeV at the 95% confidence level, where a limit of 54 GeV is expected. In cases in which either the observed limit or the expected limit is obtained just before the inaccessible region, the difference between the observed and expected limit may become large, if one of them is beyond and the other

just before the inaccessible region. If for example in Figure 4b, the cross-section was slightly higher such that it was just above the observed cross-section limit and it crossed the expected limit at 90 GeV, the expected limit on m_h would have been at 90 GeV and the observed limit would have been beyond the inaccessible region which would yield a limit larger than 100 GeV. This leads to the large steps in Figure 6.

The same procedure was performed to find the lowest allowed mass of the radion-like state, m_r . The result of the scan in the $\xi - \Lambda_W$ plane is shown in Figures 5c and d. The cross-section of the radion-like state vanishes for large negative mixing and decreases rapidly with increasing Λ_W , since the couplings of the radion to SM particles is proportional to the inverse of Λ_W . The analyses lose their sensitivity for $\Lambda_W \gtrsim 0.8$ TeV and for maximal negative mixing; therefore, a mass limit independent of the mixing parameter ξ cannot be extracted.

4 Summary

Limits on the Higgsstrahlung cross-section obtained from data recorded with the OPAL detector have been used to restrict the parameter space of the Randall-Sundrum model. The data exclude masses for the Higgs-like state below 58 GeV for all scales $\Lambda_W \geq 246$ GeV, independent of the mixing between the radion and the Higgs boson, and of the radion mass. The analyses are sensitive to the radion for scales $\Lambda_W \lesssim 0.8$ TeV. No universal limit, independent of Λ_W , ξ and m_h , on the mass of the radion-like state can be extracted.

Acknowledgements

We particularly wish to thank Laura Covi, Csaba Csáki, Graham D. Kribs, Thomas G. Rizzo and James Wells for their support. We also thank the SL Division for the efficient operation of the LEP accelerator at all energies and for their close cooperation with our experimental group. In addition to the support staff at our own institutions we are pleased to acknowledge the

Department of Energy, USA,

National Science Foundation, USA,

Particle Physics and Astronomy Research Council, UK,

Natural Sciences and Engineering Research Council, Canada,

Israel Science Foundation, administered by the Israel Academy of Science and Humanities,

Benoziyo Center for High Energy Physics,

Japanese Ministry of Education, Culture, Sports, Science and Technology (MEXT) and a grant under the MEXT International Science Research Program,

Japanese Society for the Promotion of Science (JSPS),

German Israeli Bi-national Science Foundation (GIF),

Bundesministerium für Bildung und Forschung, Germany,

National Research Council of Canada,

Hungarian Foundation for Scientific Research, OTKA T-038240, and T-042864,

A Appendix

A.1 Physical Scalars in the RS-Model

In [?], the effective 4D Lagrangian is derived, which describes the kinetic terms of the radion and the Higgs boson and their couplings to SM particles. Starting from the effective Lagrangian, the physical states and their masses are computed as shown in [?], and the radion-like and Higgs-like states are defined.

The following kinetic terms for the radion \tilde{r} and the Higgs boson \tilde{h} have been found:

$$\mathcal{L}_{\text{scalar}} \simeq \begin{pmatrix} \tilde{h} \\ \tilde{r} \end{pmatrix}^T \begin{pmatrix} -\frac{1}{2}\square - \frac{1}{2}\tilde{m}_h^2 & 3\xi\gamma\square \\ 3\xi\gamma\square & -\frac{1}{2}(1 + 6\xi\gamma^2)\square - \frac{1}{2}\tilde{m}_r^2 \end{pmatrix} \begin{pmatrix} \tilde{h} \\ \tilde{r} \end{pmatrix}, \quad (2)$$

where ξ is a free parameter of $\mathcal{O}(1)$, leading to the kinetic mixing between the radion and the Higgs boson. The normalisation of the radion field depends on $\gamma = v/\sqrt{6}\Lambda_W$, where v is the vacuum expectation value of the Higgs field and Λ_W the mass scale on the SM brane. The values \tilde{m}_r and \tilde{m}_h are fundamental mass parameters of the radion and the Higgs fields.

The physical states are obtained by diagonalisation of the matrix in Equation (2) [?]. First the kinetic mixing is resolved by the choice $\tilde{h} = h' + 6\xi\gamma r'/Z$ and $\tilde{r} = r'/Z$, with:

$$Z = \sqrt{1 + 6\xi\gamma^2(1 - 6\xi)}. \quad (3)$$

The fields, h' and r' , are real i.e. physical scalars only if:

$$\frac{1}{12} \left(1 - \sqrt{1 + \frac{4}{\gamma^2}} \right) < \xi < \frac{1}{12} \left(1 + \sqrt{1 + \frac{4}{\gamma^2}} \right). \quad (4)$$

The choice of h' and r' removes the kinetic mixing, but introduces a mixing of the mass terms for non zero \tilde{m}_r and \tilde{m}_h . The matrix of the mass terms is diagonalised by rotating by the angle θ :

$$\tan 2\theta = 12\xi\gamma Z \frac{\tilde{m}_h^2}{\tilde{m}_r^2 - \tilde{m}_h^2(Z^2 - 36\xi^2\gamma^2)}. \quad (5)$$

The canonically normalised kinetic terms of the fields h' and r' are invariant under rotations. The full transformation yields the following relations between the fundamental states, \tilde{h} and \tilde{r} , and the mass eigenstates, \hat{h} and \hat{r} :

$$\begin{aligned} \tilde{h} &= \left(\cos\theta - \frac{6\xi\gamma}{Z} \sin\theta \right) \hat{h} + \left(\sin\theta + \frac{6\xi\gamma}{Z} \cos\theta \right) \hat{r} \\ \tilde{r} &= -\sin\theta \frac{\hat{h}}{Z} + \cos\theta \frac{\hat{r}}{Z}. \end{aligned} \quad (6)$$

The corresponding masses are given by m_{\pm} , where $m_- \leq m_+$ ($m_- = m_+$ for $\xi = 0$ and $\tilde{m}_r = \tilde{m}_h$):

$$m_{\pm}^2 = \frac{1}{2Z^2} \left(\tilde{m}_r^2 + (1 + 6\xi\gamma^2)\tilde{m}_h^2 \pm \sqrt{(\tilde{m}_r^2 - \tilde{m}_h^2(1 + 6\xi\gamma^2))^2 + 144\gamma^2\xi^2\tilde{m}_r^2\tilde{m}_h^2} \right). \quad (7)$$

For $\xi = 0$, m_+ is the mass of the mass eigenstate \hat{h} if $\tilde{m}_h > \tilde{m}_r$ (otherwise this is the mass of the eigenstate \hat{r}). The assignment of m_{\pm} to the eigenstates \hat{r} and \hat{h} changes at the poles, ξ_0 , of (5): $\tilde{m}_r = \tilde{m}_h(Z^2 - 36\xi_0^2\gamma^2)$. Here, the rotation angle θ flips by $\pi/2$. For $|\xi| > |\xi_0|$, \hat{h} becomes eigenstates with mass m_- if $\tilde{m}_h > \tilde{m}_r$ (otherwise of the eigenstate \hat{r}).

In the following, the radion-like and Higgs-like state, r and h , are defined such that for $\xi = 0$ the fundamental radion \tilde{r} and the mass eigenstate r coincide, and furthermore, the mass m_r and the couplings (see Section A.2) are continuous functions of ξ . The definition of r is:

$$r = \begin{cases} \hat{r} & \text{if } (\tilde{m}_r > \tilde{m}_h \text{ and } \xi^2 < \frac{\tilde{m}_h Z^2 - \tilde{m}_r}{36\gamma^2\tilde{m}_h}) \\ & \text{or } (\tilde{m}_r \leq \tilde{m}_h \text{ and } \xi^2 \geq \frac{\tilde{m}_h Z^2 - \tilde{m}_r}{36\gamma^2\tilde{m}_h}) \\ \hat{h} & \text{otherwise} \end{cases}. \quad (8)$$

The corresponding mass is $m_r = m_-$ if $\tilde{m}_r \leq \tilde{m}_h$ and $m_r = m_+$ if $\tilde{m}_r > \tilde{m}_h$. The Higgs-like state and its mass are defined accordingly. The masses are shown in Figure 1a as a function of ξ for fundamental radion and Higgs boson mass parameters \tilde{m}_r and \tilde{m}_h of 90 GeV and 120 GeV.

Equations (7) can be solved for \tilde{m}_r and \tilde{m}_h :

$$\begin{aligned} \tilde{m}_r^2 &= \frac{Z^2}{2} \left((m_+^2 + m_-^2) \pm \sqrt{(m_+^2 - m_-^2)^2 - \frac{144\xi^2\gamma^2}{Z^2} m_+^2 m_-^2} \right) \\ \tilde{m}_h^2 &= \frac{Z^2}{2(1 + 6\xi\gamma^2)} \left((m_+^2 + m_-^2) \mp \sqrt{(m_+^2 - m_-^2)^2 - \frac{144\xi^2\gamma^2}{Z^2} m_+^2 m_-^2} \right). \end{aligned} \quad (9)$$

The signs have to be chosen such that $m_r(\xi = 0) = \tilde{m}_r$ and $m_h(\xi = 0) = \tilde{m}_h$. The computed masses \tilde{m}_r and \tilde{m}_h are real only if:

$$\frac{m_+^2}{m_-^2} \geq \frac{1}{Z^2} \left(1 + 6\xi\gamma^2(1 + 6\xi) + 12\gamma\sqrt{\xi^2(6\xi\gamma^2 + 1)} \right). \quad (10)$$

This condition, together with (4), limits the possible physical parameters as illustrated in Figure 1b.

A.2 Couplings of the Higgs Boson and Radion to SM Particles

The couplings of the radion-like and the Higgs-like states, which are defined in the Appendix A.1, are extracted applying the methods of [?]. In contrast to [?], the physical states are derived from the effective Lagrangian of [?], which is a higher order approximation.

The radion couples to the trace of the energy-momentum tensor T_μ^μ [?]; therefore, the couplings to matter are similar to those of the SM Higgs boson at lowest order since:

$$T_\mu^\mu = -(m_{ij}\bar{\psi}_i\psi_j - m_V V_\mu V^\mu) + \dots, \quad (11)$$

where ψ_i and V_μ denote fermions and bosons, m_{ij} and m_V their masses. The contribution of terms with derivatives of fields or more than two fields is negligible here. The combined interaction term of the radion and the Higgs boson is:

$$\mathcal{L}_{\text{radion/Higgs inter.}} \simeq -\frac{1}{v}(m_{ij}\bar{\psi}_i\psi_j - m_V V_\mu V^\mu) [\tilde{h} - \gamma\tilde{r}], \quad (12)$$

where v denotes the vacuum expectation value of the Higgs field. The couplings of the radion to the fermions and bosons are generally reduced by the factor $\gamma = v/\sqrt{6}\Lambda_W$ compared to the corresponding couplings of the Higgs boson.

The couplings of the radion-like and the Higgs-like state r and h are obtained by inserting (6) according to (8) into (12) and comparing the resulting terms with the Higgs interaction terms of the SM Lagrangian. This yields for the radion-like state, expressed in terms of the partial decay width relative to the one of the SM Higgs boson¹:

$$k_f = k_V = \frac{\Gamma(r \rightarrow \bar{f}f)}{\Gamma(\text{H}_{\text{SM}} \rightarrow \bar{f}f)} = \frac{\Gamma(r \rightarrow VV)}{\Gamma(\text{H}_{\text{SM}} \rightarrow VV)} = (a_{1,r} + a_{2,r})^2, \quad (13)$$

where

$$a_{i,r} = \begin{cases} a_{i,\tilde{r}} & \text{if } (\tilde{m}_r > \tilde{m}_h \text{ and } \xi^2 < \frac{\tilde{m}_h Z^2 - \tilde{m}_r}{36\gamma^2 \tilde{m}_h}) \\ & \text{or } (\tilde{m}_r \leq \tilde{m}_h \text{ and } \xi^2 \geq \frac{\tilde{m}_h Z^2 - \tilde{m}_r}{36\gamma^2 \tilde{m}_h}) \\ a_{i,\tilde{h}} & \text{otherwise} \end{cases}. \quad (14)$$

The relative decay width of the Higgs-like state is given by (13) replacing $a_{i,r}$ by $a_{i,h}$, where $a_{i,h}$ is defined accordingly. The following relations for $a_{i,\tilde{r}}$ and $a_{i,\tilde{h}}$ are obtained:

$$\begin{aligned} a_{1,\tilde{r}} &= \sin\theta + \frac{6\xi\gamma}{Z} \cos\theta & a_{2,\tilde{r}} &= \gamma \frac{\cos\theta}{Z} \\ a_{1,\tilde{h}} &= \cos\theta - \frac{6\xi\gamma}{Z} \sin\theta & a_{2,\tilde{h}} &= \gamma \frac{\sin\theta}{Z}. \end{aligned} \quad (15)$$

Expression (13) is valid for all fermions f and massive vector bosons V at lowest order.

In case the Higgs boson or radion is lighter than two times the top mass, m_t , direct decays into top quarks are kinematically forbidden, but due to the large mass of the top quark, decays into gluons via top loops are generally not negligible. The matrix element of a SM Higgs boson decay into gluons is:

$$\text{ME}(\text{H}_{\text{SM}} \rightarrow gg) = \frac{1}{2} \cdot \frac{\alpha_s}{8\pi} \cdot \frac{1}{v} \text{H}_{\text{SM}}(x) F_{\frac{1}{2}}(4m_t^2/m_{\text{H}_{\text{SM}}}^2) G_{\alpha\mu\nu}(x) G_\alpha^{\mu\nu}(x). \quad (16)$$

The strong coupling constant is denoted by α_s , the Higgs boson mass by $m_{\text{H}_{\text{SM}}}$ and the gluon fields by $G_{\alpha\mu\nu}$. The function $F_{\frac{1}{2}}$ is the form factor of the top loop, which is defined by [?]:

$$F_{\frac{1}{2}}(\tau) = -2\tau [1 + (1 - \tau)f(\tau)], \quad (17)$$

¹For a given mass m_r (m_h) the expression has to be evaluated using a mass $m_{\text{H}_{\text{SM}}} = m_r$ ($m_{\text{H}_{\text{SM}}} = m_h$).

where

$$f(\tau) = \begin{cases} \arcsin^2 \frac{1}{\sqrt{\tau}}, & \text{if } \tau \geq 0 \\ -\frac{1}{4} \left[\ln \frac{1+\sqrt{1-\tau}}{1-\sqrt{1-\tau}} - i\pi \right]^2, & \text{if } \tau < 0. \end{cases} \quad (18)$$

A similar matrix element is obtained for the radion, however it has the opposite sign and the coupling is reduced by γ . Since the radion couples to the trace of the energy momentum tensor, the anomaly of the trace contributes to the decay width into gluons and photons in addition to the loop contribution. The anomalous terms appear in the trace of the renormalised energy momentum tensor in addition to the unrenormalised trace \tilde{T}_μ^μ . This has been shown for example in [?]. The complete trace T_μ^μ reads:

$$T_\mu^\mu = \tilde{T}_\mu^\mu + \frac{\beta}{2g_R} N[F_{\alpha\lambda\rho} F_\alpha^{\lambda\rho}], \quad (19)$$

where g_R denotes the renormalised coupling constant, β the renormalisation group coefficient, $F_\alpha^{\mu\nu}$ the field strength tensor of strong, electromagnetic and weak interaction and $N[\dots]$ normal ordering. Thus, the radion couples directly to gluon and photon pairs due to the trace anomaly. The additional coupling to the massive vector bosons is negligible. To fully describe the coupling of the radion to gluon pairs, the matrix element $\text{ME}(r \rightarrow gg)$ equivalent of (16) has to be extended with the term:

$$\text{ME}_{\text{anomaly}}(r \rightarrow gg) = \beta \cdot (\alpha_s/8\pi) \gamma r(x) G_{\alpha\mu\nu}(x) G_\alpha^{\mu\nu}(x). \quad (20)$$

For the SU(3) group of QCD, the renormalisation group coefficient $\beta=7$. In total, the partial decay width of the radion-like state becomes [?]:

$$k_g = \frac{\Gamma(r \rightarrow gg)}{\Gamma(\text{H}_{SM} \rightarrow gg)} = \frac{\left| 2 \cdot \beta \cdot a_{2,r} - (a_{1,r} + a_{2,r}) F_{\frac{1}{2}}(4m_t^2/m_r^2) \right|^2}{\left| F_{\frac{1}{2}}(4m_t^2/m_r^2) \right|^2}. \quad (21)$$

The factors $a_{i,r}$ are those of (14). The partial decay width of the Higgs-like state, $\Gamma(h \rightarrow gg)$ is given by (21) replacing $a_{i,r}$ by $a_{i,h}$, and m_r by m_h .

Except for the additional coupling to gluon pairs and scaled coupling strength, the couplings of the radion-like and the Higgs-like states are the same as those of the SM Higgs boson. Thus in e^+e^- collisions at centre-of-mass energies achieved at LEP, the mass eigenstates, $\varphi = r$ or h , are dominantly produced in the Higgsstrahlung process, $e^+e^- \rightarrow Z^* \rightarrow Z\varphi$. The total decay width of the mass eigenstates is smaller than 100 MeV for masses of interest ($m_\varphi \lesssim 115$ GeV). Thus only decays, $Z^* \rightarrow Z\varphi$, into on-shell Higgs bosons or radions have to be considered. The cross-section relative to Higgsstrahlung in the SM is derived from (13) and given by:

$$\frac{\sigma(e^+e^- \rightarrow Z\varphi)}{\sigma(e^+e^- \rightarrow Z\text{H}_{SM}; m_{\text{H}_{SM}} = m_\varphi)} = \frac{\Gamma(\varphi \rightarrow VV)}{\Gamma(\text{H}_{SM} \rightarrow VV)}. \quad (22)$$

In Figure 2, the cross-section and branching ratios of the two mass eigenstates are displayed as a function of the mixing parameter ξ . Due to the contribution from the trace anomaly, the radion decays predominantly into a pair of gluons.

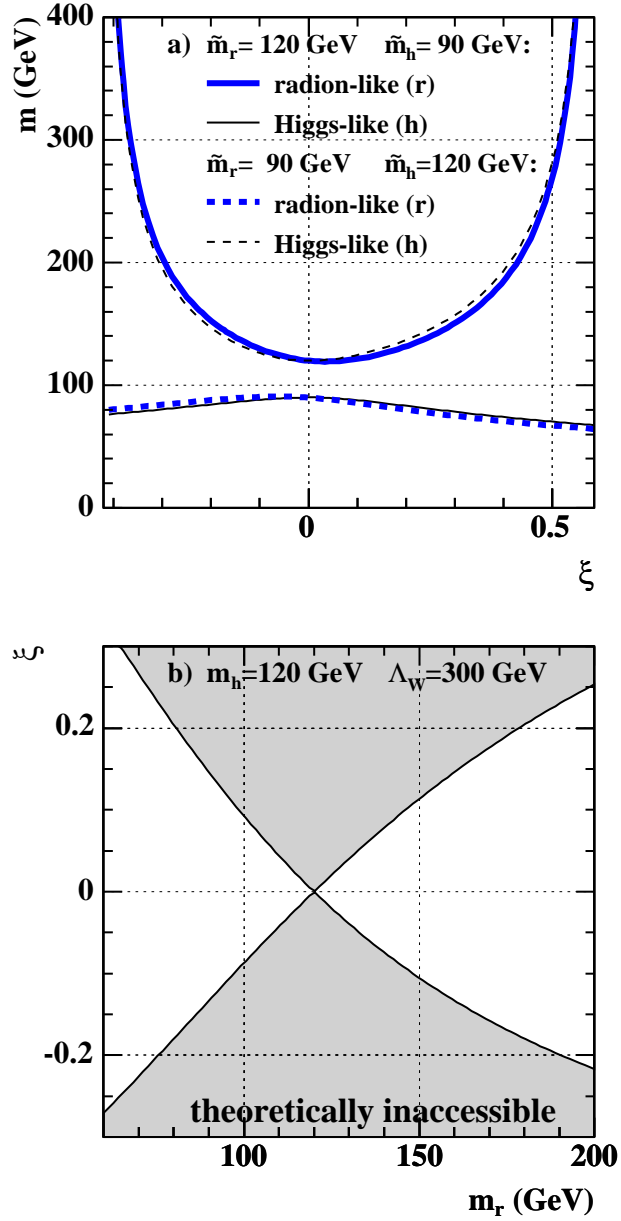


Figure 1: a) Masses $m_{r/h}$ of the heavy and light mass eigenstates for fundamental Higgs boson and radion mass parameters, \tilde{m}_h and \tilde{m}_r , of 90 GeV and 120 GeV. The fundamental radion is chosen to be heavier (lighter) than the Higgs boson, indicated by the solid (dashed) lines. The x -axis extends over the allowed ξ -range. b) Allowed parameter space in the m_r and ξ plane for a Higgs boson mass $m_h = 120$ GeV. Outside the permitted region the Higgs and radion-like states are unphysical (ghost-like). In both figures the weak scale was chosen to be $\Lambda_W = 300$ GeV.

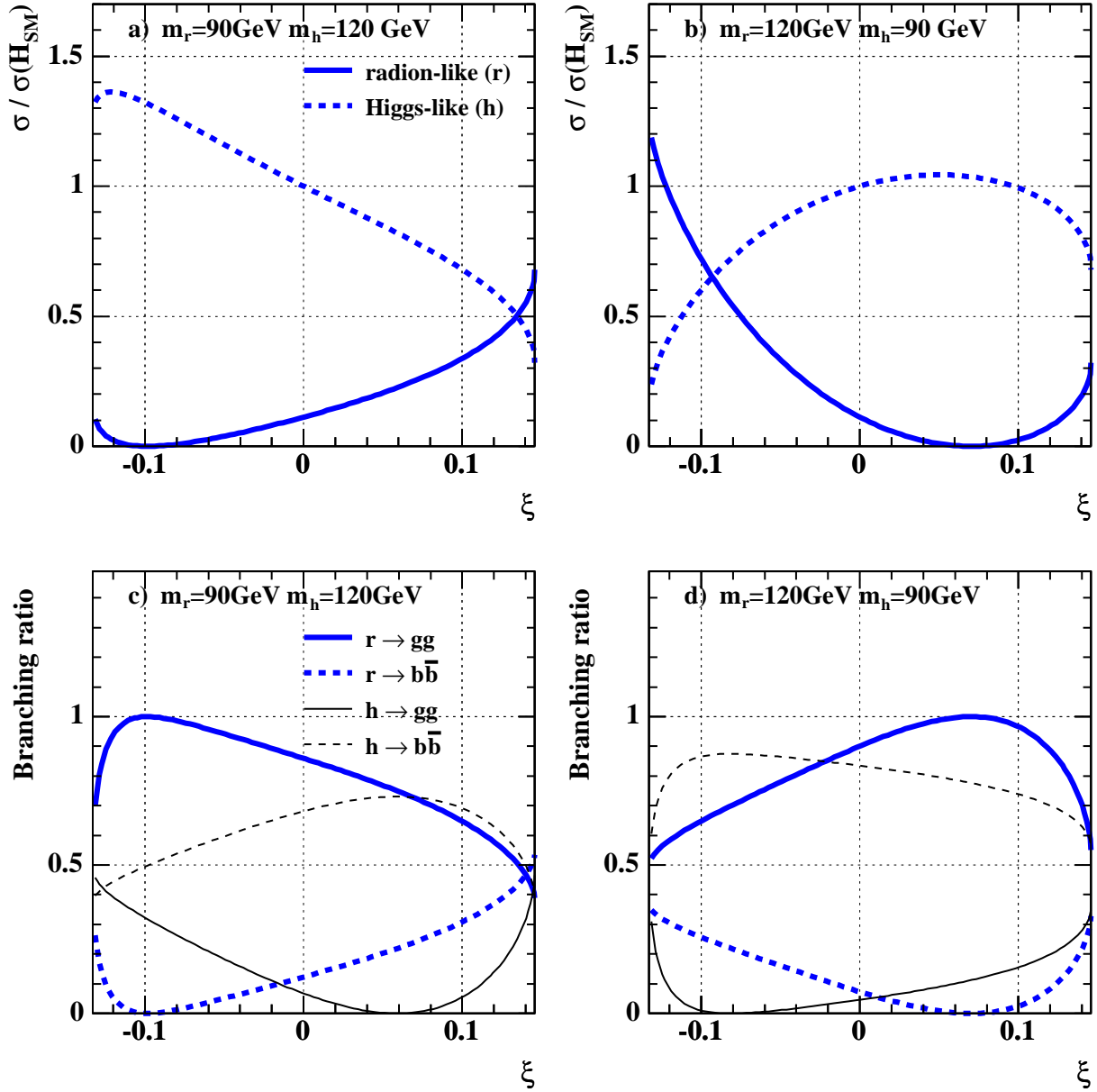


Figure 2: a) and b) the cross-sections for the processes $e^+e^- \rightarrow Zr$ or Zh of the radion-like and the Higgs-like state, r and h , relative to the corresponding cross-section for a SM Higgs boson for two different values of m_r and m_h . c) and d) the branching ratios of r and h into gluon pairs and $b\bar{b}$. The parameter Λ_W was chosen to be 300 GeV. The cross-sections and branching ratios of the Higgs-like state h are identical to those of a SM Higgs boson for $\xi = 0$.

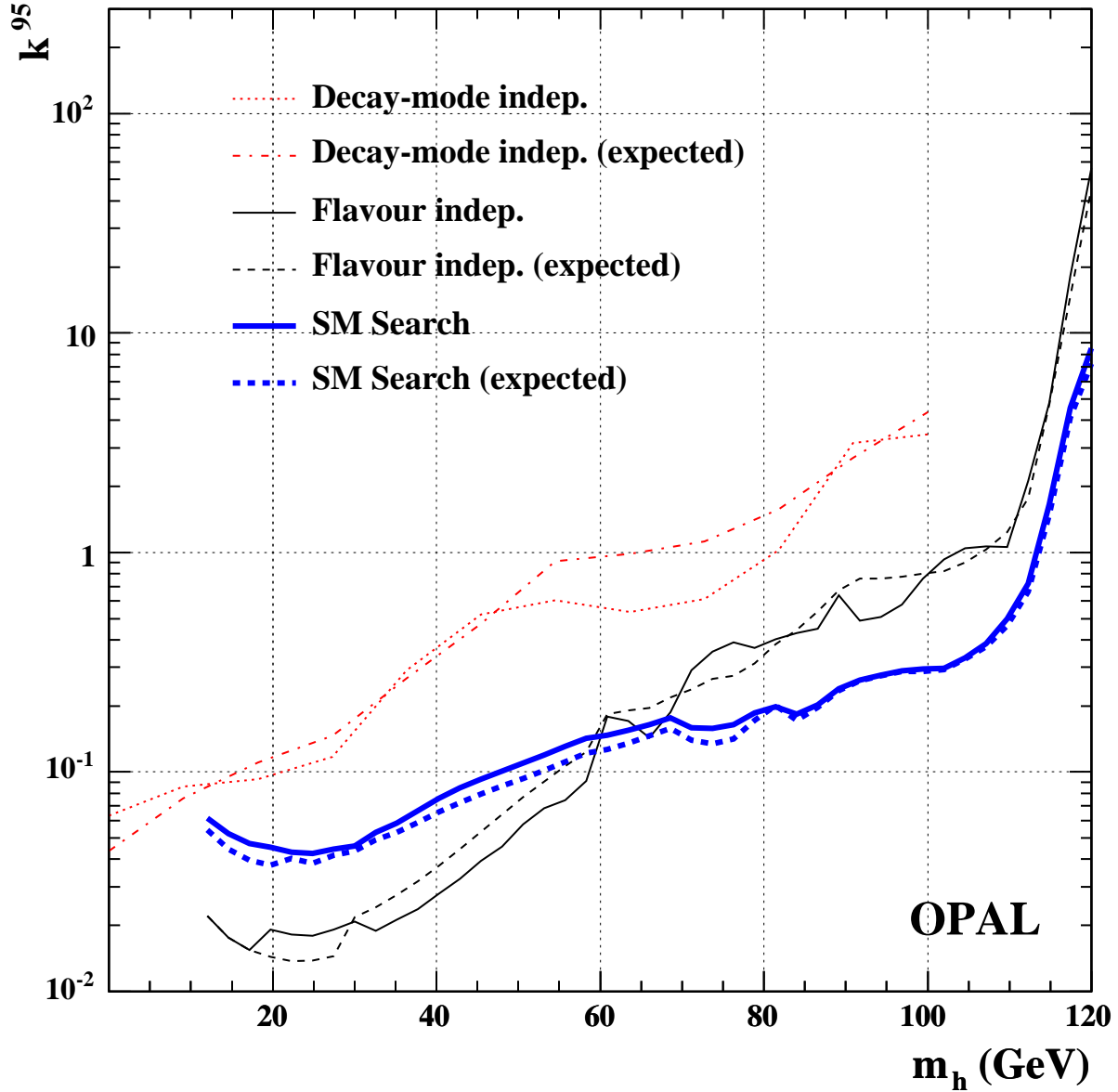


Figure 3: The observed and expected limits on the scale factor k as a function of the Higgs boson mass obtained by the SM Higgs boson search, the flavour independent and the decay-mode independent Higgs boson search. The scale factor k relates the cross-section times branching ratio to the cross-section of SM Higgsstrahlung. The limits equally apply to the radion-like and the Higgs-like state of the Randall-Sundrum model each with the mass m_h .

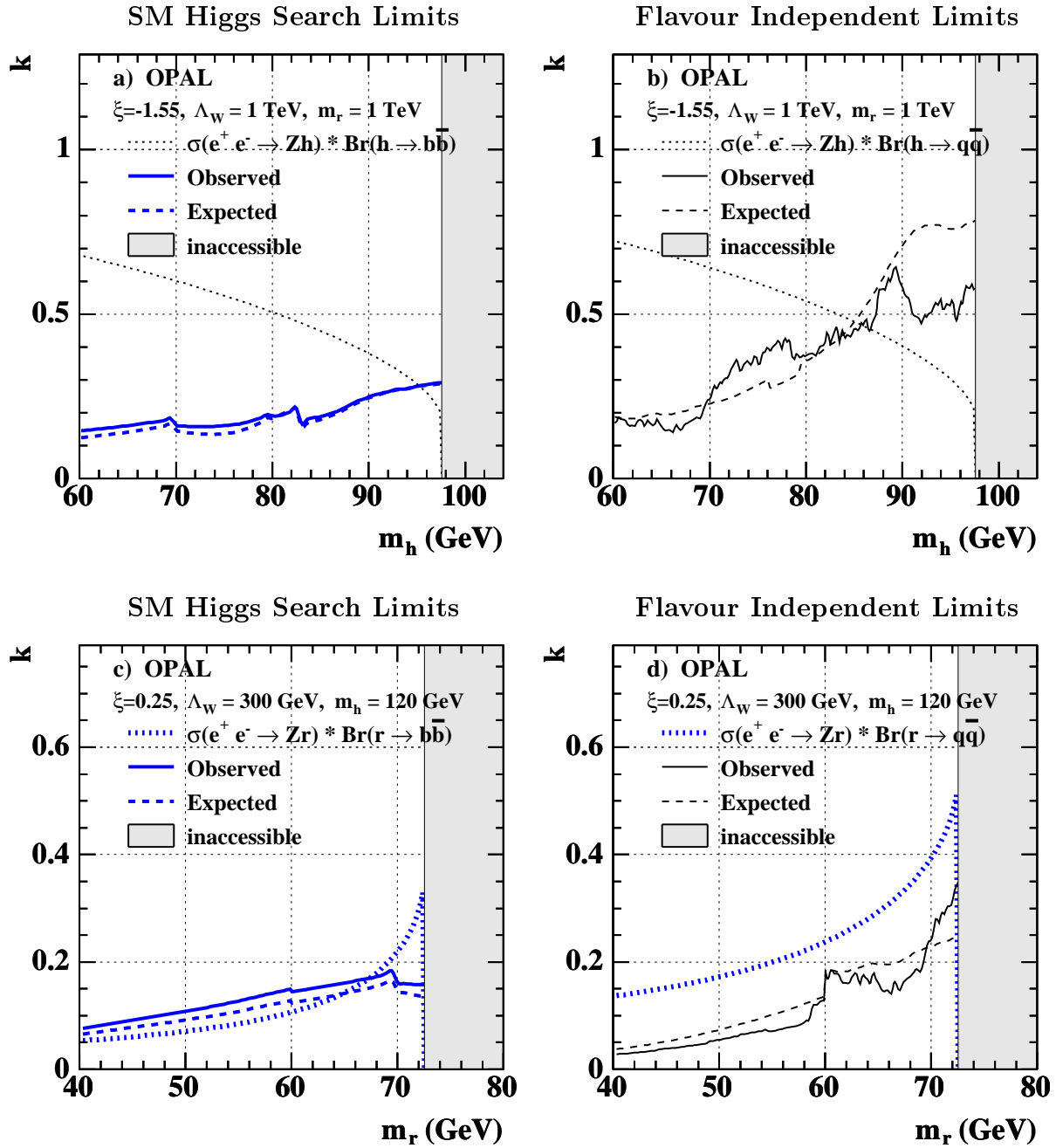


Figure 4: The cross-section times branching ratio of the Higgs-like (Figure a and b) and radion-like state (Figure c and d) relative to the cross-section of SM Higgsstrahlung together with the observed and expected limits (solid and dashed lines) obtained from the SM (Figure a and c) and the flavour independent (Figure b and d) Higgs boson searches at one point in the Randall-Sundrum parameter space as a function of the mass of the Higgs-like state m_h and the mass of the radion-like state m_r . The dotted lines in Figures a and c indicate the cross-section times $Br(r \text{ or } h \rightarrow b\bar{b})$ and in Figures b and d the cross-section times $Br(r \text{ or } h \rightarrow \text{hadrons})$. The shaded region is inaccessible by the theory. Model points are excluded if the predicted cross-section times branching ratio exceeds the limit.

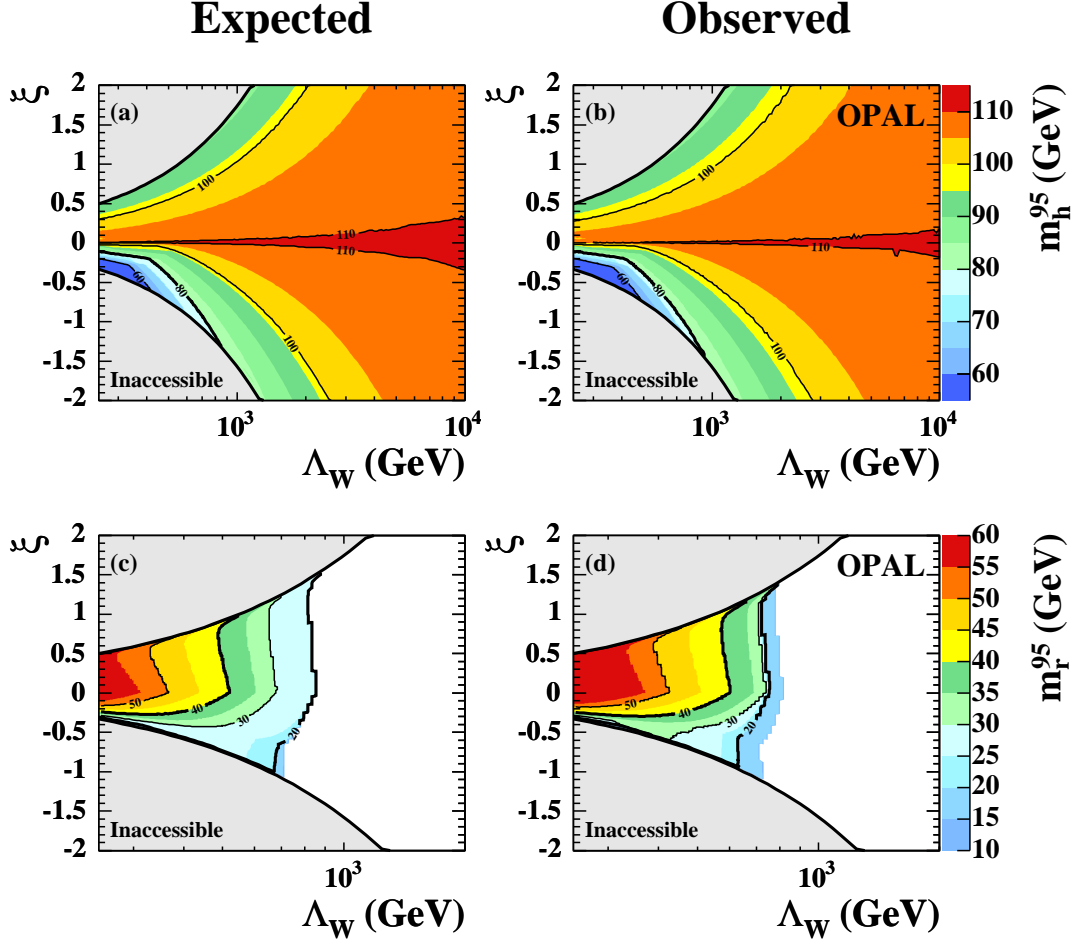


Figure 5: Expected and observed lower limits on the mass of the Higgs-like and the radion-like state, m_h (a and b) and m_r (c and d), as a function of the mixing parameter ξ and the scale parameter Λ_W . The Figures a) and c) show the expected limit, and Figures b) and d) the observed limit. Inside each shaded region, the obtained lower mass limit is equal or larger than the value indicated by the code on the right. The regions in the upper and lower left corner are inaccessible by the theory.

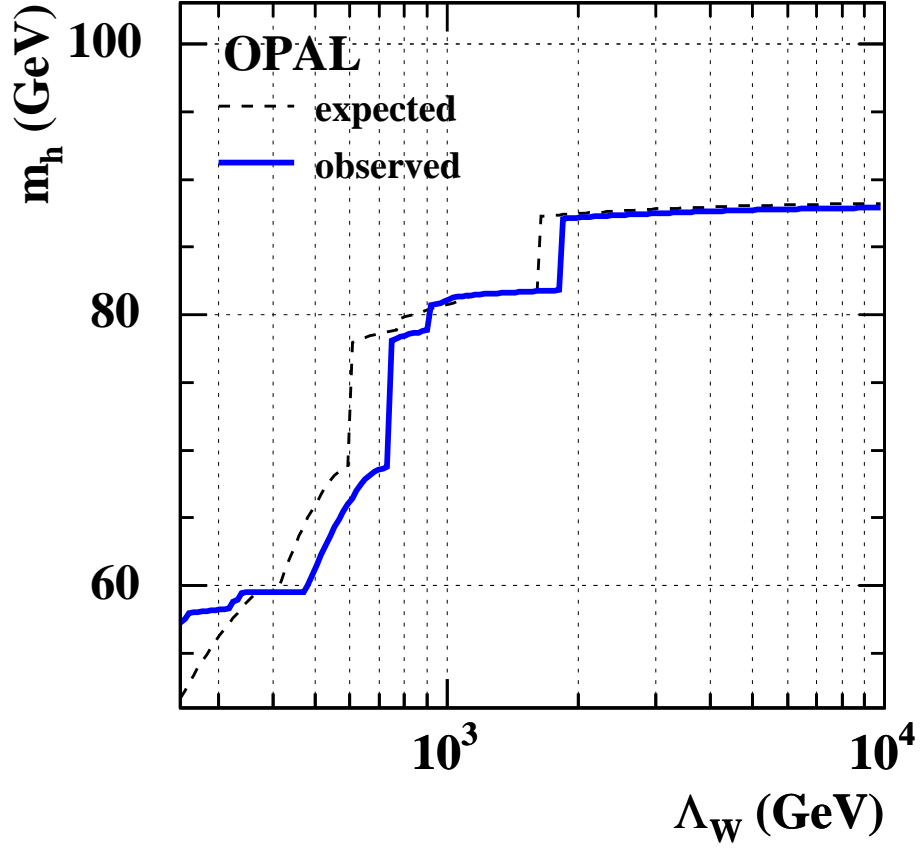


Figure 6: The lowest expected and observed limit on the Higgs boson mass as a function of the scale parameter Λ_W for all allowed ξ and for masses of the radion-like state m_r in the range from 1 MeV to 1 TeV. The analyses often lose their sensitivity close to the inaccessible region. If the region up to the inaccessible region is covered, the next allowed mass will be several GeV further away. This causes the step like structure.